

Kinetic-energy structure of a laser-produced-plasma channel in airXiao-Fang Shu,¹ Cheng-Xin Yu,² Wei Li,³ and Shi-Bing Liu^{1,*}¹*Institute of Laser Engineering, Beijing University of Technology, Beijing, 100124, China*²*Institution of Applied Physics and Computational Mathematics, Beijing 100088, China*³*China Academy of Space Technology, Beijing Institute of Space Mechanics and Electricity, Beijing 100094, China*

(Received 17 September 2015; published 29 December 2015)

In this paper, we propose a method to calculate the fine structure of kinetic energy of laser-produced plasma, which bridges the two parts of researches of plasma channel usually studied independently of each other, i.e., the extension of the length of plasma filament and the prolongation of the lifetime of plasma channel generated by the laser pulse. The kinetic energy structure of the plasma channel is calculated by solving the motion equation of ionized electrons and utilizing the ionization rate as the weighting factor. With the study on the laser intensity, we analyze the formation mechanisms of the kinetic energy structure. This work holds great promise for optimizing the initial conditions of the evolutions of plasma channel after the laser pulse.

DOI: [10.1103/PhysRevA.92.063844](https://doi.org/10.1103/PhysRevA.92.063844)

PACS number(s): 42.65.Sf, 42.65.Jx, 52.50.-b, 52.38.Hb

I. INTRODUCTION

When intense femtosecond pulses propagate in air, filamentation takes place as long as the Kerr self-focusing effect balances the diffraction and plasma defocusing [1]. To maintain this balance the filament needs to consume its own energy and is expected to vanish eventually once its power falls below a certain threshold, leaving one or more conducting plasma channels in the wake of the pulse. This plasma channel in air holds the promise of potential for many applications, such as THz radiation sources [2,3], spectral manipulations of the laser pulse [4,5], remote radiation sources and triggering [6–9], and guiding of electrical discharges [10–13], which has drawn much attention from a large number of researchers.

There are mainly two aspects of research that people are truly interested in about the filamentation in air: one is to extend the length of plasma filament and the other is to prolong the lifetime of laser-produced plasma (LPP) after the laser pulse. These two studies are usually carried out separately. Extending the plasma channel is usually realized by choosing appropriate configurations of incident pulses and adjusting parameters of applied lenses, such as using a single-step phase plate [14], nondiffraction Bessel beams [15–17], and ring-Gaussian beam [18]. Recently, Scheller and his colleagues used a secondary low-intensity annular “dressing beam,” which is focused by a conical axicon, to continuously refuel the optical filament [19]. In the study on the lifetime of plasma channel, the initial distributions of plasma density and temperature are selected artificially most of the time. For instance, people directly use Maxwellian distribution as the initial electron energy distribution [20,21], which considerably simplifies the situation and the calculations but therefore leads to some considerable inaccuracy of the LPP evolution. Here the nonlinear optical interaction is local and assumed to be instantaneous, which makes the distribution of velocity and energy become very intractable.

Control of the key characters of the plasma filaments, for instance, the diameter, length, starting position, density, and temperature distribution, etc., is of great importance to most of

the possible applications. The experiments such as lightning discharge guidance and remote sensing of the atmosphere critically depend on the information of the plasma channel, thereby resulting in a necessity to investigate the evolution of the plasma channel left behind by the laser pulses [1,22].

The aim of this work is to connect the two separate studies by proposing a method to calculate the kinetic energy distribution of the plasma channel left after the laser pulse. Together with the density distribution, the nonequilibrium initial conditions of plasma channel evolution is given. This approach not only gives more details and insights into understanding of the fundamentals of filamentation but also offers a viable route to calculating and simulating its evolution.

This paper is organized as follows. In Sec. II, we present the theoretical scheme to calculate the kinetic energy distribution of the LPP channel in air. Then the kinetic energy structure of LPP for Gaussian-shape strong laser pulses and the corresponding generation mechanisms are discussed in Sec. III. The summaries of our work are given in Sec. IV.

II. THEORETICAL MODELS

The propagation of intense femtosecond laser pulses in air involves a great number of nonlinear effects such as diffraction, self-focusing, group-velocity dispersion (GVD), as well as plasma generation and energy losses due to multiphoton ionization. By employing the slowly varying envelope approximation, the filamentation process in our simulation is governed by a generalized nonlinear Schrödinger equation in a moving coordinate system $\xi = z, \tau = t - z/v_g$ as [23,24]

$$\begin{aligned} \frac{\partial \mathcal{E}}{\partial \xi} = & \frac{i}{2k_0} \nabla_{\perp}^2 \mathcal{E} - \frac{i\beta_2}{2} \frac{\partial^2}{\partial \tau^2} \mathcal{E} + \frac{ik_0 n_2}{2} |\mathcal{E}|^2 \mathcal{E} \\ & - \frac{ik_0 \rho_e}{2 \rho_c} \mathcal{E} - \frac{\beta^{(K)}}{2} |\mathcal{E}|^{2K-2} \mathcal{E}, \end{aligned} \quad (1)$$

where v_g is the group velocity of the laser pulse and k_0 the wave number. On the right-hand side of Eq. (1), the first term describes the diffraction of the laser beam with the transverse Laplacian $\nabla_{\perp}^2 = \frac{1}{r} \frac{\partial}{\partial r} (r \frac{\partial}{\partial r})$. The second term means the group-velocity dispersion with coefficient β_2 , and the third represents

*Corresponding author: sbliu@bjut.edu.cn

the Kerr self-focusing of the driving laser field, in which n_2 is the nonlinear refractive index. The fourth term characterizes the acceleration of the LPP driven by the laser field, where ρ_e is the transient density of the LPP and ρ_c the critical density. The fifth term is responsible for the ionization loss due to the K -photon ionization of air with the coefficient $\beta^{(K)}$. Since the applied pulse is on the order of femtoseconds, the Raman effects are omitted here.

Neglecting the impact ionization and electron-ion recombination for femtosecond durations [24–26], the transient plasma density $\rho_e(\tau)$ is given by $\rho_e(\tau) = \rho_0 \{1 - \exp[-\int_{-\infty}^{\tau} W(\tau') d\tau']\}$, where ρ_0 is the initial number density of neutral molecules. In the multiphoton ionization regime, the ionization rate of air molecules is $W(\tau) = \frac{\beta^{(K)}}{K \hbar \omega_0} |\mathcal{E}(\tau)|^{2K}$ [26], where $\omega_0 = k_0 c$ is the central angular frequency of the laser field whose propagation speed is the same as that of light in vacuum c , and \hbar is the reduced Planck constant.

As we know, Eq. (1) describes the evolution of the envelope of intense femtosecond pulse. However, for the ionized electrons quivering in the laser field, they are sensitive to the temporal profile of the laser pulse. So there is a need for us to retrieve the fast oscillation of the laser pulse in order to investigate the dynamics of the LPP. Considering the fast varying components, the laser field used is written as

$$\mathbf{E}(\tau) = \sqrt{\frac{2}{\varepsilon_0 c}} \mathcal{E}(\tau) e^{i\omega_0 \tau}, \quad (2)$$

where ε_0 is the dielectric constant. As an example, we present the normalized laser field for a Gaussian pulse in the direction of time in Fig. 1. To show the temporal profile of the laser field clearly, we zoom in the figure on the interval between $[-20, 20]$ fs in the bottom panel.

Commonly, for an ionized electron in the plasma channel produced by a femtosecond pulse, the attraction of its parent ion and the collisions with other electrons are not taken into

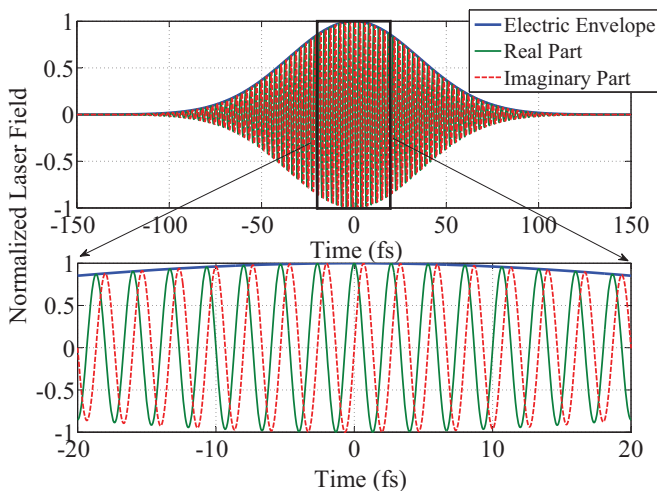


FIG. 1. (Color online) The restored laser field normalized by its electric peak strength. The blue solid line (upper curve) represents the normalized electric envelope, the green solid line is the real part of the laser field, and the red dashed line denotes the imaginary part.

account. Therefore, the dynamics of an ionized electron born at τ_0 in the dipole approximation is governed by the Newtonian equation, $m_e d\mathbf{V}(\tau_0, \tau)/d\tau = e\mathbf{E}(\tau)$, where m_e and e are the rest mass and charge of an electron, respectively. By integrating over $[\tau_0, \tau_f]$, we obtain the final velocity of the electron in terms of the electric envelope,

$$\mathbf{V}(\tau_0, \tau) = \sqrt{\frac{2}{\varepsilon_0 c}} \frac{e}{m_e} \int_{\tau_0}^{\tau_f} \mathcal{E}(\tau) e^{i\omega_0 \tau} d\tau, \quad (3)$$

where τ_f is the time when the laser pulse ends. Thus, the final kinetic energy of the ionized electron born at τ_0 can be calculated using $E_{\text{kin}}(\tau_0, \tau_f) = \frac{1}{2} m_e |\mathbf{V}(\tau_0, \tau)|^2$. For the convenience of experimental measurement, we calculate the mean kinetic energy carried by an ionized electron at τ_f as [27]

$$\langle E_{\text{kin}} \rangle = \left[\int_{-\infty}^{\tau_f} E_{\text{kin}}(\tau_0, \tau_f) \dot{\rho}_e(\tau_0) d\tau_0 \right] / \rho_e(\tau_f), \quad (4)$$

where the dot over $\rho_e(\tau_0)$ represents the first derivative with respect to τ_0 .

Due to the very low ionization degree in the LPP channel, i.e., $\rho_e/\rho_0 \leq 10^{-3}$, we can approximately write the time-dependent LPP density as

$$\rho_e(\tau) \approx \frac{\rho_0 \beta^{(K)}}{K \hbar \omega_0} \int_{-\infty}^{\tau} |\mathcal{E}(\tau')|^{2K} d\tau', \quad (5)$$

which gives the final expression of the mean kinetic energy,

$$\langle E_{\text{kin}} \rangle = \frac{e^2}{m_e \varepsilon_0 c} \times \frac{\int_{-\infty}^{\tau_f} [|\int_{\tau_0}^{\tau_f} \mathcal{E}(\tau) e^{i\omega_0 \tau} d\tau|^2] |\mathcal{E}(\tau_0)|^{2K} d\tau_0}{\int_{-\infty}^{\tau_f} |\mathcal{E}(\tau')|^{2K} d\tau'}. \quad (6)$$

The method of calculating mean kinetic energy applies to the spatial distribution of electric envelopes as well.

III. SIMULATIONS AND DISCUSSIONS

The propagation equations (1) are numerically solved by the symmetrical operator splitting method, in which the transverse evolution is calculated for a half-step using the Crank-Nicolson scheme in time domain, then, after a fast-Fourier transform of the envelope function, the evolution due to the group velocity dispersion is carried out for a half-step in frequency domain. For the nonlinear evolution (i.e., the Kerr effect, plasma defocusing and multiphoton ionization), we calculate the propagation of the pulse envelope for one step by using the iteration method twice. After that, the effects of group velocity dispersion and the transverse evolution are performed for another half-step, respectively. To investigate the fine structure of plasma channel and its kinetic energy distribution, we apply nonuniform grids in the transverse direction, where the density of grid points is higher in the vicinity of the transverse center, while coarse-grid points are distributed far from the center. One great advantage of doing this is that fewer grids are used, thereby speeding up the computation.

To start with, we simulate an incident femtosecond pulse with $\lambda_0 = 810$ nm, which means that the minimal number of photons $K = 10$ for the mean ionization potential $I_p = 14.6$ eV of air. In this situation, the ionization coefficient $\beta^{(10)} = 1.27 \times 10^{-126} \text{ cm}^{17}/\text{W}^9$ and the critical power for

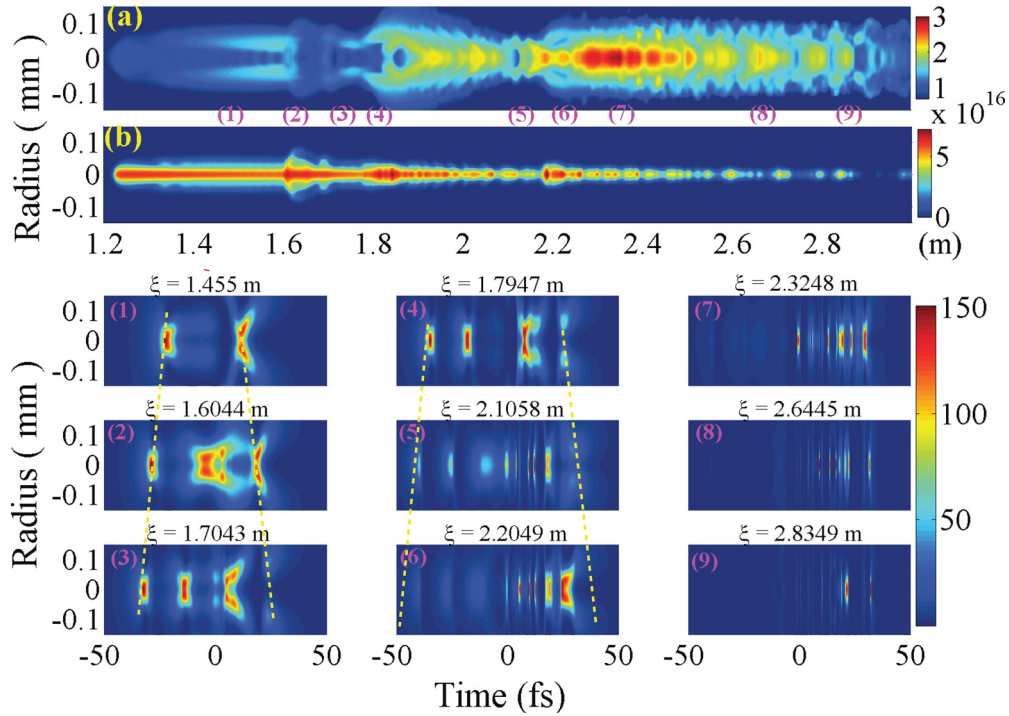


FIG. 2. (Color online) (a) Fine structure of kinetic energy of LPP in the unit of eV on a logarithmic scale; (b) the number density of LPP in the unit of cm^{-3} , where (a) and (b) share the abscissa axis (i.e., the propagation distance). To investigate the formation of kinetic energy structure and plasma channel, we select several typical positions labeled by (1)–(9) in magenta and present the corresponding laser intensity normalized by I_0 and propagation distances in the following panels, where the initial peak laser intensity is $I_0 = 2P_{\text{in}}/\pi r_p^2$. The yellow and dashed lines in (1)–(6) give the trajectories of the two initial splitting portions.

self-focusing in air at λ_0 is $P_{\text{cr}} = \lambda_0^2/2\pi n_2 \approx 3.3$ GW, where the nonlinear refractive index $n_2 = 3.2 \times 10^{-19} \text{ cm}^2/\text{W}$ [26]. Here the transverse profile is assumed to be cylindrically symmetric since only the single filament is taken into account. Without loss of generality, we write the initial electric field envelope as

$$\mathcal{E}(\xi = 0, \tau, r) = \sqrt{\frac{2P_{\text{in}}}{\pi r_p^2}} \exp\left(-\frac{\tau^2}{\tau_p^2} - \frac{r^2}{r_p^2} - \frac{ik_0 r^2}{2f}\right), \quad (7)$$

where P_{in} is the peak power of the incident femtosecond laser pulse. The parameters $\tau_p = 50$ fs and $r_p = 2$ mm are the widths at e^{-2} of the femtosecond pulse in the time and transverse directions, respectively, and $f = 2$ m is the focal length. In our simulation, the initial laser energy is $E = 2$ mJ, which gives $P_{\text{in}} \approx 12.2P_{\text{cr}}$, and the self-focusing distance [28]

$$z_f = \frac{0.367z_0}{\sqrt{[P/P_{\text{cr}} - 0.852]^2 - 0.0219 + z_0/f}} \quad (8)$$

with the Rayleigh range $z_0 = \pi n_0 r_p^2/\lambda_0$.

In Figs. 2(a) and 2(b), we present the fine structures of kinetic energy of the plasma channel on a logarithmic scale and the corresponding plasma density in the unit of cm^{-3} , respectively. According to the derivations and discussions above, we know that the generation of laser-produced plasma depends on the laser intensity, while the kinetic energy of an ionized electron is very sensitive to the temporal structure of laser electric field. Therefore, the kinetic energy structure demonstrate very different behaviors with the density of LPP

channel. In order to investigate the formation of the kinetic energy structure and the evolution of LPP density, we mark out several typical positions labeled by (1)–(9) in magenta, and the corresponding distributions of laser intensity ($|\mathcal{E}|^2$) are also shown in the three rows below in order to reveal the mechanisms of the kinetic energy structure and plasma channel.

Experiencing competitions among the Kerr effect, the transverse diffraction and the GVD effect, an intense laser pulse is focused at the distance of about $\xi = 1.25$ m, where the plasma filamentation begins, which is in agreement with the prediction by Eq. (8). We observe that the plasma channel keeps stable until $\xi \approx 1.6$ m where the laser filament splits into two distantly separated portions in the direction of the time axis, as shown in Fig. 2(1), in the transverse direction ranging from about -0.01 to 0.01 mm, the amount of time when the laser intensity almost holds still is approximately the same. As discussed above, the kinetic energy of an ionized electron depends on its generation time and the temporal structure of the laser field. The front portion of the laser pulse mainly contributes to the generation of plasma, while the rear portion is responsible for the acceleration of the generated electrons and the generation of new electrons. Considering the cylindric symmetry in the the propagation equation, we believe that the intensity distribution of the pulse rear edge in the r - τ plane [see Fig. 2(1)] causes the tubular structures of the kinetic energy. The dynamic competitions and rebalances among the transverse diffraction, plasma defocusing, and Kerr self-focusing lead to the ladder structure inside the tube of kinetic energy between positions (1) and (2) in Fig. 2(a).

While the laser pulse travels in air, the two separated portions continue moving toward the front and rear edges, respectively, and a new portion peeps out near $t = 0$ fs due to the refocusing of the front portion. After that the new portion splits into two parts moving away from each other, which is known as the generation of multiple filaments in the direction of the time axis (see Ref. [29]).

From Fig. 2(2), we can see that the newly formed portions distribute in a larger region in contrast to the two former portions, which leads to the generation of more electrons as shown in location (2) in Fig. 2(a). But the multiple filamentation disrupts the acceleration of the LPP to some extent. As a consequence, the kinetic energy of LPP is considerably lower in the region between locations (2) and (3). In the same way, the low intensity near the axis and the high intensity far from the axis at the rear edge of the laser pulse once again causes the tubular structure of kinetic energy, which is shown between (3) and (4) in Fig. 2(a). Then the splitting two front parts of the laser pulse will cause the pulse to split into more fragments, and these new portions also undergo splitting. Because of the generations of LPP via multiphoton ionization and refocusing via Kerr effects (i.e., energy transfer), the front portions gradually decay with time. In Figs. 2(1)–2(6), we also plot the trajectories of the two initially formed portions with yellow and dashed lines. Compared with acceleration of LPP, the multiphoton ionization plays a major role in the laser energy losses, which manifests as the fading of the front portions in Figs. 2(4)–2(9). The evolution of the kinetic energy structure of LPP can be analyzed in the same way. It can be clearly seen that the maximal averaged kinetic energy is about 0.82 keV, appearing at position (7) in Fig. 2(a). The corresponding laser intensity distribution is shown in Fig. 2(7).

The energy density of the plasma channel after the laser pulse given as the product of LPP density at τ_f and the averaged kinetic energy per electron, $\mathcal{P}_E(\xi, r) = \rho_e(\tau_f) \langle E_{\text{kin}} \rangle$, has a great influence on the evolution and lifetime of the plasma channel. In Fig. 3, we present the simulation results

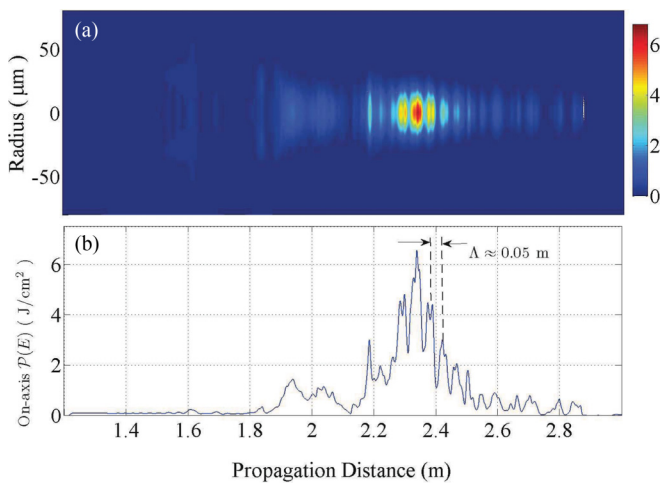


FIG. 3. (Color online) (a) The kinetic energy density of the plasma channel in the unit of J/cm^3 after the laser pulse; (b) the values of on-axis kinetic energy density, in which the quasiperiodic structure of kinetic energy density is observed between $\xi \approx 2.1$ –2.7 m with a cycle length $\Lambda \approx 0.05$ m.

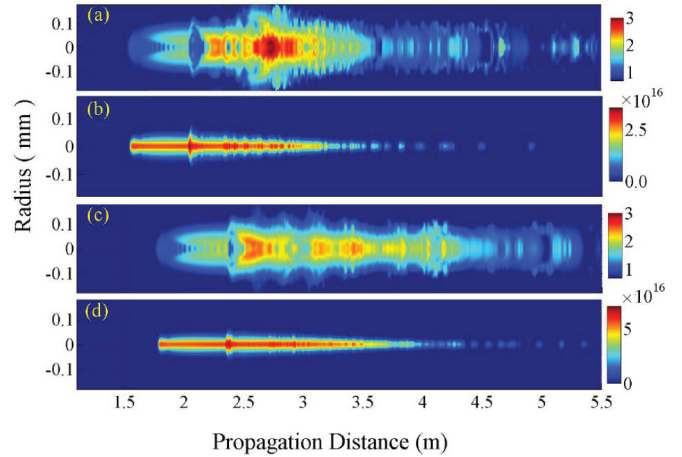


FIG. 4. (Color online) The dependence of FKSE and LPP density on the focusing length f . (a) and (b) $f = 3$ m; [(c) and (d)] $f = 4$ m.

on a linear scale rather than the logarithmic scale used in Fig. 2(a). Figure 3(a) clearly shows that, with a lower density ($\leq 0.2 \text{ J}/\text{cm}^3$), the kinetic energy density has a tubular and ladder structure similar to kinetic energy structure in the left. It can also be observed that the energy mainly distributes in the region $\xi = 2.2$ –2.5 m. In Fig. 3(b), we give the values of energy density for $r = 0$, which has a quasiperiodic structure with a cycle length $\Lambda \approx 0.05$ m between $\xi \approx 2.1$ and 2.7 m. The quasiperiodic structure of energy density also reflects the dynamic evolution of the temporal structure of laser pulse.

In order to reveal the dependence of the kinetic energy structure on the focusing length f , we perform the numerical calculations in cases of $f = 3$ and 4 m, respectively, as shown in Fig. 4. Using Eq. (8), the starting position of the plasma channel is evaluated as $z_f \approx 1.6$ m for $f = 3$ m and $z_f \approx 1.8$ m for $f = 4$ m, which is consistent with the simulation results. Obviously, the kinetic energy structure and the LPP density with the focusing length $f = 3$ and 4 m validate our aforementioned analysis and discussions. From Figs. 4(b) and 4(d), the profile of LPP density almost remains the same when $f = 2, 3$, and 4 m. As presented in Figs. 4(a) and 4(c), the tubular and ladder structures can also be seen in the left part of the kinetic energy structure. Note that the low-energy region on the right of the tubular structure has a shorter range with $f = 3$ m [see Fig. 4(a)] than that with $f = 2$ m [see Fig. 2(a)], and for $f = 4$ m, there is only a bubble in the low-energy region, as shown in Fig. 4(d).

To reveal the dependence of kinetic energy structure on focusing length, we choose the maximal value of the mean kinetic energy per electron for each propagation distance as

$$E_m(\xi) = \max_{r \in [0, R]} [\langle E_{\text{kin}}(r, \xi) \rangle],$$

where R is the maximal transverse range of the laser beam. The comparison of the results with three different focusing lengths is given in Fig. 5. For the focusing length $f = 2$ m, the high kinetic energy (i.e., the high temperature) mainly distributes in $\xi \approx 2.3$ –2.4 m (the blue line) while the plasma channel ranges from about $\xi \approx 1.2$ to 2.9 m [see Fig. 2(b)]. In the case of $f = 3$ m, the region of high kinetic energy lies in the range $\xi \approx 2.6$ –2.9 m with the peak value $\max[E_m] \approx 1.1$ keV (the green line)

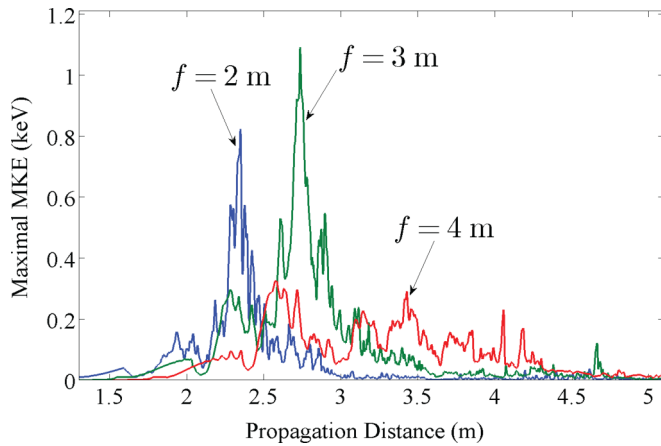


FIG. 5. (Color online) The transverse maximal values of the mean kinetic energy versus the propagation distance for three different focusing length. Compared with the cases of focusing lengths $f = 2$ and 3 m, the maximum of mean kinetic energy distributes over a larger distance at a relatively uniform value (the red line).

at $\xi \approx 2.72$ m, while the plasma channel begins at $\xi \approx 1.6$ and ends at $\xi \approx 4$ m. The kinetic energy distribution for $f = 4$ m shows a comparative uniformity, which extends from $\xi \approx 2.1$ to 4.3 m at the value of about 0.1 keV (the red line).

Since the temperature and the density of plasma are two key parameters in characterizing the decay of plasma channel, the investigations on the lifetime of plasma channel are usually carried out by presupposing some initial distributions [20] or diagnosing their lifetime by means of experimental tools [21,30]. Our work bridges the generation and the decay of the laser-produced plasma channel by extracting information about the dynamics of the electrons, in which the kinetic energy [see Eq. (6)] and density of LPP can be used as the

initial conditions for the evolution and decay of the plasma channel after the laser pulse. And, hopefully, the optimized parameters of incident laser pulses and applied lenses can be obtained by balancing the extension of plasma filament and the prolongation of the lifetime of the plasma channel.

IV. CONCLUSIONS

To summarize, we derive the mean kinetic energy of the LPP by retrieving the fast oscillating factor of the laser field and solving the motion equation of ionized electrons, which connects the researches of extending the length of plasma filament and prolonging the lifetime of LPP after the laser pulse. Considering the tenuity of the air and the low degree of LPP, we neglect the collisions of ionized electrons with other electrons and ions and describe the motion of an ionized electron using the Newtonian equation. Using the ionization rate as the weighting factor, we obtain the kinetic energy distribution of the LPP at the end of the laser pulse, which is directly related to the temperature distribution of the plasma channel.

Later, we simulate a Gaussian-shaped strong laser pulse passing through a convex lens with a focusing length f and then propagating in air. By numerically solving Eq. (1) and calculating the mean kinetic energy (6), we obtain the density and the kinetic energy distribution of LPP. With the study on the laser intensity distribution in the r - τ plane, we analyze the formation mechanisms of the kinetic energy structure. We also compare the simulation results for three different focusing lengths, $f = 2, 3$, and 4 , and discuss the dependence of kinetic energy structure on the parameters of the applied lens. This work is expected to provide a effective method of obtaining the optimal conditions for plasma channel evolution.

ACKNOWLEDGMENT

This work was supported by the NSAF of China (Grant No. U1530153).

-
- [1] A. Couairon and A. Mysyrowicz, *Phys. Rep.* **441**, 47 (2007).
 - [2] C. D'Amico, A. Houard, M. Franco, B. Prade, A. Mysyrowicz, A. Couairon, and V. T. Tikhonchuk, *Phys. Rev. Lett.* **98**, 235002 (2007).
 - [3] C. D'Amico, A. Houard, S. Akturk, Y. Liu, J. Le Bloas, M. Franco, B. Prade, A. Couairon, V. T. Tikhonchuk, and A. Mysyrowicz, *New J. Phys.* **10**, 013015 (2008).
 - [4] K. Stelmaszczyk, P. Rohwetter, G. Méjean, J. Yu, E. Salmon, J. Kasparian, R. Ackermann, J. P. Wolf, and L. Wöste, *Appl. Phys. Lett.* **85**, 3977 (2004).
 - [5] H. L. Xu, G. Méjean, W. Liu, Y. Kamali, J. F. Daigle, A. Azarm, P. T. Simard, P. Mathieu, G. Roy, J. R. Simard, and S. L. Chin, *Appl. Phys. B* **87**, 151 (2007).
 - [6] J. F. Gravel, Q. Luo, D. Boudreau, X. P. Tang, and S. L. Chin, *Anal. Chem.* **76**, 4799 (2004).
 - [7] P. Rairoux, H. Schillinger, S. Neirdeimer, M. Rodriguez, F. Ronneberger, R. Sauerbrey, B. Stein, D. Waite, C. Wedekind, H. Wille, L. Wöste, and C. Ziener, *Appl. Phys. B: Lasers Opt.* **71**, 573 (2000).
 - [8] J. Kasparian, M. Rodriguez, G. Méan, J. Yu, E. Salmon, H. Wille, R. Bourayou, S. Frey, Y. B. André, A. Mysyrowicz, R. Sauerbrey, J. P. Wolf, and L. Wöste, *Science* **301**, 61 (2003).
 - [9] Q. Luo, H. L. Xu, S. A. Hosseini, J. F. Daigle, F. Théberge, M. Sharifi, and S. L. Chin, *Appl. Phys. B* **82**, 105 (2006).
 - [10] J. Kasparian, R. Ackermann, Y. André, G. Méchain, G. Méjean, B. Prade, P. Rohwetter, E. Salmon, K. Stelmaszczyk, J. Yu, A. Mysyrowicz, R. Sauerbrey, L. Wöste, and J. Wolf, *Opt. Express* **16**, 5757 (2008).
 - [11] X. M. Zhao, J. C. Diels, C. Y. Wang, and J. M. Elizondo, *IEEE J. Quantum Electron.* **31**, 599 (1995).
 - [12] S. L. Chin and K. Miyazaki, *Jpn. J. Appl. Phys.* **38**, 2011 (1999).
 - [13] R. Ackermann, K. Stelmaszczyk, P. Rohwetter, G. Mejean, E. Salmon, J. Yu, J. Kasparian, G. Mechain, V. Bergmann,

- S. Schaper, B. Weise, T. Kumm, K. Rethmeier, W. Kalkner, L. Wöste, and J. P. Wolf, *Appl. Phys. Lett.* **85**, 5781 (2004).
- [14] Y. Fu, H. Xiong, H. Xu, J. Yao, B. Zeng, W. Chu, Y. Cheng, Z. Xu, W. Liu, and S. Chin, *Opt. Lett.* **34**, 3752 (2009).
- [15] J. Durnin, *J. Opt. Soc. Am. A* **4**, 651 (1987).
- [16] J. Durnin, J. J. Miceli, and J. H. Eberly, *Phys. Rev. Lett.* **58**, 1499 (1987).
- [17] P. Polynkin, M. Kolesik, A. Roberts, D. Faccio, P. D. Trapani, and J. Moloney, *Opt. Express* **16**, 15733 (2008).
- [18] Z. F. Feng, W. Li, C. X. Yu, X. Liu, J. Liu, and L. B. Fu, *Phys. Rev. A* **91**, 033839 (2015).
- [19] M. Scheller, M. S. Mills, M. A. Miri, W. Cheng, J. V. Moloney, M. Kolesik, P. Polynkin, and D. N. Christodoulides, *Nat. Photon.* **8**, 297 (2014).
- [20] S. Bodrov, N. Aleksandrov, M. Tsarev, A. Murzanev, I. Kochetov, and A. Stepanov, *Phys. Rev. E* **87**, 053101 (2013).
- [21] S. Bodrov, V. Bukin, M. Tsarev, A. Murzanev, S. Garnov, N. Aleksandrov, and A. Stepanov, *Opt. Express* **19**, 6829 (2011).
- [22] S. L. Chin, S. A. Hosseini, W. Liu, Q. Luo, F. Théberge, N. Aközbek, A. Becker, V. P. Kandidov, O. G. Kosareva, and H. Schroeder, *Can. J. Phys.* **83**, 863 (2005).
- [23] S. Skupin, L. Bergé, U. Peschel, and F. Lederer, *Phys. Rev. Lett.* **93**, 023901 (2004).
- [24] T. T. Xi, X. Lu, and J. Zhang, *Phys. Rev. Lett.* **96**, 025003 (2006).
- [25] L. Berge, S. Skupin, F. Lederer, G. Méjean, J. Yu, J. Kasparian, E. Salmon, J. P. Wolf, M. Rodriguez, L. Wöste, R. Bourayou, and R. Sauerbrey, *Phys. Rev. Lett.* **92**, 225002 (2004).
- [26] S. Tzortzakis, L. Bergé, A. Couairon, M. Franco, B. Prade, and A. Mysyrowicz, *Phys. Rev. Lett.* **86**, 5470 (2001).
- [27] X. F. Shu and S. B. Liu, *Appl. Phys. B* **120**, 697 (2015).
- [28] J. H. Marburger, *Prog. Quantum Electron.* **4**, 35 (1975).
- [29] See Supplemental Material at <http://link.aps.org/supplemental/10.1103/PhysRevA.92.063844> for the evolution of laser profile and the corresponding kinetic energy structure of plasma channel for different propagation distance.
- [30] X. Lu, S. Y. Chen, J. L. Ma, L. Hou, G. Q. Liao, J. G. Wang, Y. J. Han, X. L. Liu, H. Teng, H. Han, Y. T. Li, L. M. Chen, Z. Y. Wei, and J. Zhang, *Sci. Rep.* **5**, 15515 (2015).